Vol.3, No.3, Page 885- 890, 2025 https://doi.org/10.59628/jast.v3i3.1761 ISSN 2958-9568 JAST

SUN PUBLISHER

مجلة جامعة صنعاء للعلوم التطبيقية والتكنولوجيا

Sana'a University Journal of Applied Sciences and Technology

https://journals.su.edu.ye/index.php/jast/

Enhanced Focus Shaping of Circularly Polarized Laguerre–Gaussian Vortex Beams Using a Binary Axicon

Hassan T. Al-Ahsab [1,2,3], Mingjian Cheng [2], Ibrahim G. H. Loqman [1], Shukri Kaid [1,4] and Abdu A. Alkelly [1*]

[1]**Department of Physics, Faculty of Science, Sana'a University, Sana'a, Yemen,**
[2]**School of Physics, Xidian University, Xi'an 710071, China,**
[3]**Physics Department, Faculty of Applied Science, Thamar University, Thamar, Yemen,**
[4]**Physics Department, Faculty of Science, Taiz University, Taiz, Yemen.**

*Corresponding author: a.alkelly@su.edu.ye

Abstract

The focus shaping of light beams is crucial for a range of optical applications, including trapping, imaging, and material processing. In this work, based on the vector diffraction theory, the focus shaping of a circularly polarized Laguerre–Gaussian vortex beam by a binary axicon was investigated. By analyzing the effects of beam parameters such as order p, topological charge m, truncation parameter β, and optical system characteristics including obstruction δ and NA, this study demonstrates how these factors influence the focal intensity distribution. By appropriately choosing specific parameters, different focal shapes, such as multifoci and double spots, were formed in the focal region of the binary axicon. The findings underscore the potential of binary axicons as versatile tools for advanced focus engineering in optical trapping and particle manipulation.

Article Info

Keywords:
Focus shaping, Laguerre–Gaussian vortex beam,Binary axicon, Vector diffraction theory, Circular polarization

Article History:
Received: 4-May-2025,
Revised: 28-May-2025,
Accepted: 3-June-2025,
Available online: 30-June-2025.

1. INTRODUCTION

Vortex beams, distinguished by their helical phase fronts, inherently carry orbital angular momentum (OAM), and the phase structure is expressed as $\exp(im\varphi)$, where m denotes the topological charge (or quantum number), and φ represents the azimuthal angle [1–3]. Laguerre–Gaussian vortex (LGV) beams, a prominent class of vortex beams, are distinguished by their radial and azimuthal indices, (p, m), which define their unique intensity and phase structures. For $m \neq 0$, LGV beams exhibit a distinctive doughnut-shaped intensity profile featuring $(p+1)$ concentric rings and circular–cylindrical symmetry [4]. These unique characteristics have enabled their application in diverse fields, including optical communication [5, 6], rotational motion detection [7], perfect vortex beam generation [8], particle trapping [9–11], and focus-shaping [12–14].

Circularly polarized vortex beams further combine OAM with spin angular momentum (SAM), thereby significantly enhancing their functionality and expanding their application potential [15–19]. Focus shaping of these beams involves engineering the intensity, phase, and polarization distribution at the focal plane through advanced optical elements, such as spatial light modulators, q-plates, or metasurfaces, which enables the generation of customized optical structures including tightly focused spots, flat-topped beams, two-petal laser beams, spiral spin density vectors, and multiple optical bottle beams [20–26]. Circularly polarized Laguerre–Gaussian vortex (CPLGV) beams, in particular, have shown remarkable performance in cutting-edge applications, such as trapping and manipulation of particles [27, 28], particle acceleration [29, 30], and optical communication [6].

Axicons, which are optical elements that transform an incident beam into an extended focal line rather than a conventional focal spot, have emerged as powerful tools in beam shaping and have been widely used in numerous fields owing to their exceptional properties [20, 21, 31–33]. Un-

like traditional lenses, axicons generate a conical wavefront, resulting in a depth of focus significantly longer than that produced by spherical lenses [31, 34]. For example, linear axicons have been widely employed to generate Bessel-like beams and to create specialized focal shapes [14, 31, 35], double focal spots [32], and flat-topped beams [36]. Beyond linear axicons, various advanced designs have been developed to enhance their capabilities further, such as axicon doublets [37], spiral axicons [20, 21, 38] and binary axicons [21, 39, 40]. Binary axicons, formed by combining defocusing and focusing linear axicons, offer additional flexibility, facilitating the creation of photonic nanohelices [41], polarization transformations [21], formation of double-ring intensity patterns [39], and extension of focal depth [40]. Owing to their ability to engineer complex focal fields and control polarization states, binary axicons offer a versatile platform for tailoring the focal properties of CPLGV beams beyond traditional optical systems [21, 40, 41]. Despite their significant potential, the focus shaping of CPLGV beams through binary axicons remains unexplored to the best of our knowledge. Investigating the interplay between the intrinsic characteristics of CPLGV beams and the spatial structuring capabilities of binary axicons is of considerable scientific and practical interest with implications for next-generation optical trapping, sensing, and communication technologies.

In this article, we study the focus-shaping of circularly polarized Laguerre–Gaussian vortex beams using a binary axicon, employing Richards and Wolf vectorial diffraction theory. In Section 2, we present a detailed theoretical framework for calculating the intensity distribution of circularly polarized Laguerre–Gaussian vortex beams focused on a binary axicon. Section 3 provides numerical simulations of the intensity distribution of left-hand CPLGV beams in the focal region and explores the influence of varying beam and optical system parameters. Finally, in Section 4, we summarize our findings and present our concluding remarks.

2. THEORETICAL FRAMEWORK

The electric field of a circularly polarized Laguerre (LG) vortex beam at the input pupil is expressed as follows [15]:

$$\mathbf{E}^{\pm}(\theta,\varphi) = A(\theta)\frac{\mathbf{e}_x \pm i\mathbf{e}_y}{\sqrt{2}}\exp[im\varphi], \tag{1}$$

where $A(\theta)$ denotes the amplitude distribution, $\mathbf{e}_x$ and $\mathbf{e}_y$ are unit vectors along the x- and y-directions, respectively, $\pm$ indicates left-hand $(+)$ or right-hand $(-)$ circular polarization, and m is the topological charge representing the orbital angular momentum (OAM) of the beam.

Using vector diffraction theory, the electric field in the focal region of a tightly focused circularly polarized LG beam is given by [42]

$$\mathbf{E}^{\pm}(\rho,\phi,z) = \begin{bmatrix} E_x^{\pm}(\rho,\phi,z) \\ E_y^{\pm}(\rho,\phi,z) \\ E_z^{\pm}(\rho,\phi,z) \end{bmatrix} = -\frac{if}{\lambda}\int_{\sigma*\alpha}^{\alpha}\int_0^{2\pi}\sqrt{\cos\theta} \times \sin\theta A(\theta,\varphi)\mathbf{P}^{\pm}(\theta,\varphi)T(\theta) \times \exp[ik(z\cos\theta + \rho\sin\theta\cos(\varphi-\phi))]\,d\varphi\,d\theta, \tag{2}$$

where the polarization vector $\mathbf{P}(\theta,\varphi)$ is given by

$$\mathbf{P}^{\pm}(\theta,\varphi) = \frac{1}{\sqrt{2}}\begin{bmatrix} 1+\cos^2\varphi R(\theta) \pm i\cos\varphi\sin\varphi R(\theta) \\ \cos\varphi\sin\varphi R(\theta) \pm i[1+\sin^2\varphi R(\theta)] \\ -\sin\theta\exp[\pm i\varphi] \end{bmatrix}, \tag{3}$$

where $R(\theta) = (\cos\theta - 1)$.

In this context, (ρ,ϕ,z) denotes the cylindrical coordinates in the focal region, $\alpha = \arcsin(NA/n_m)$ is the convergence angle defined by the numerical aperture NA and refractive index n_m of the surrounding medium. Parameter σ represents the annular obstruction, (θ,φ) refers to the spherical coordinates at the output pupil, $k = 2\pi/\lambda$ is the wave number corresponding to the wavelength λ, and f denotes the focal length.

For LGV beams with a radial index p, the pupil apodization function $A(\theta,\varphi)$ is defined as:

$$A(\theta,\varphi) = E_0\left(\sqrt{2}\beta\frac{\sin\theta}{\sin\alpha}\right)^m L_p^m\left[2\left(\beta\frac{\sin\theta}{\sin\alpha}\right)^2\right] \times \exp\left[-\left(\beta\frac{\sin\theta}{\sin\alpha}\right)^2\right]\exp[im\varphi], \tag{4}$$

where E_0 represents the amplitude constant and β refers to the truncation parameter, defined as the ratio of the pupil radius to the beam waist, where β must be greater than 1 to achieve effective beam truncation. The generalized Laguerre polynomial L_p^m corresponds to radial mode p and order m. When $p = m = 0$, Eq. 4 can be simplified to a Gaussian beam. However, for $p > 0$, the beam formed $p+1$ concentric rings. For instance, when $p = 1$, a double-ring beam is generated, which has been utilized in various applications such as creating 3D optical cages [43], 3D optical spots [44], generating double focal spots [32], and producing flat-topped beams [45], among others. These effects can be achieved by precisely adjusting both the beam parameters and the optical system configuration.

The complex transmission function $T(\theta)$ of a binary axicon is given by [21]

$$T(\theta) = \exp[i\arg(\cos(k\alpha_0 f\sin\theta))], \tag{5}$$

where α_0 is the axicon parameter. In the first diffraction order, this can be approximated as the superposition of the focusing and defocusing linear axicons [21].

$$\begin{aligned} T(\theta) &\approx \cos(k\alpha_0 f\sin\theta) \\ &= 0.5[\exp(ik\alpha_0 f\sin\theta) + \exp(-ik\alpha_0 f\sin\theta)] \end{aligned} \tag{6}$$

By applying integral identities [46],

$$\int_0^{2\pi} \cos(n\theta_1)\exp[i\eta\cos(\theta_1-\theta_2)]\,d\theta_1 = 2\pi i^n \cos(n\theta_2)J_n(\eta), \tag{7}$$

$$\int_0^{2\pi} \sin(n\theta_1)\exp[i\eta\cos(\theta_1-\theta_2)]\,d\theta_1 = 2\pi i^n \sin(n\theta_2)J_n(\eta), \tag{8}$$

The electric field components in the focal region are:

$$E_x^{\pm}(\rho,\phi,z) = -\frac{i^{m+1}kf}{\sqrt{2}}\exp[im\phi]\int_{\sigma\times\alpha}^{\alpha}\sqrt{\cos\theta}\sin\theta A(\theta) \times T(\theta)\left[J_m(k\rho\sin\theta)+\frac{(\cos\theta-1)}{2}G_{m,-}^{\pm}(\rho,\theta)\right] \times\exp[ikz\cos\theta]\,d\theta, \tag{9a}$$

$$E_y^{\pm}(\rho,\phi,z) = -\frac{i^{m+1}kf}{\sqrt{2}}\exp[im\phi]\int_{\sigma\times\alpha}^{\alpha}\sqrt{\cos\theta}\sin\theta A(\theta) \times T(\theta)\left[\pm iJ_m(k\rho\sin\theta)\pm i\frac{(\cos\theta-1)}{2}G_{m,+}^{\pm}(\rho,\theta)\right] \times\exp[ikz\cos\theta]\,d\theta, \tag{9b}$$

$$E_z^{\pm}(\rho,\phi,z) = -\frac{i^{m+1}kf}{\sqrt{2}}\exp[im\phi]\int_{\sigma\times\alpha}^{\alpha}\sqrt{\cos\theta}\sin\theta A(\theta) \times T(\theta)\left(\mp i\exp[\pm i\phi]\sin\theta J_{m\pm1}(k\rho\sin\theta)\right) \times\exp[ikz\cos\theta]\,d\theta, \tag{9c}$$

where:

$$G_{m,-}^{\pm}(\rho,\theta) = J_m(k\rho\sin\theta)-\exp[\pm i2\phi]J_{m\pm2}(k\rho\sin\theta), \tag{10}$$

$$G_{m,+}^{\pm}(\rho,\theta) = J_m(k\rho\sin\theta)+\exp[\pm i2\phi]J_{m\pm2}(k\rho\sin\theta). \tag{11}$$

The total intensity is computed as $|\mathbf{E}_t|^2 = |E_x|^2 + |E_y|^2 + |E_z|^2$. According to these equations, the focal field depends on the incident polarization state, topological charge m, truncation parameter scaling parameter β, and optical system parameters.

3. NUMERICAL CALCULATION AND DISCUSSIONS

In this section, we extensively investigate the focus-shaping of left-handed CPLGV beams focused by a binary axicon based on Eq. 9. We assume $\lambda = 632.8$ nm, $n_m = 1$, $f = 25$ mm , $\beta = 1.1, \alpha_0 = 0.0001, \delta = 0.50$, and NA $= 0.80$, unless stated otherwise.

Fig. 1 illustrates the total intensity distribution of left–handed CPLGV beams focused by the binary axicon for topological charge $m = -2:2$ and beam orders of $p = 0, 1, 2$ and 3. One can see that Uniquely focal shapes are generated in the focal region of the binary axicon with varying values of m and p. For $m = 0$, the on-axis intensity is present because of the missing phase singularity of the focused beam, which causes the presence of a Bessel function of zero order in the integrand in Eq. 9. In addition, for $m = -1$, E_z component has an on-axis intensity owing to the increasing OAM of the focused beam to 0, transforming from the SAM. Furthermore, zero on-axis intensity is formed in the case of $m = 1$ and 2 when the focus width is expanded as m increases for positive values and decreases for negative values of less than -2. These changes correspond to the formation of a focal shape as p varies. At the source plane, CPLGV beams are formed of $p + 1$ rings, resulting in changes in the focus shaping by considering the effects of other parameters, such as obstacles, δ, and the value of the truncation parameter, β. Therefore, the binary axicon allows one to obtain different focal shapes, which may find applications in the manipulation and trapping of particles.

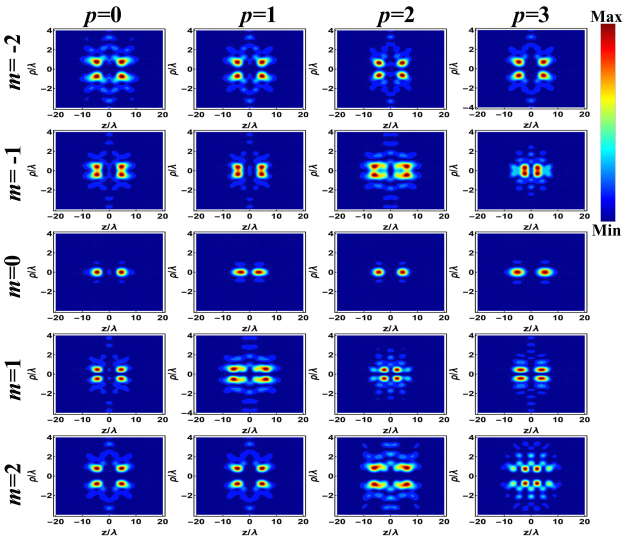

Figure 1. Intensity distribution of the left–handed CPLGV focused beams $|\mathbf{E}_t|^2$ in $\rho - z$ plane with different values of beam order p and topological charge m.

Fig. 2 shows the total intensity distribution, its components in $\rho - z$ plane and the intensity in $x - y$ plane with its phase for the z–component at $z = -5\lambda, 0$ and 5λ of left–handed CPLGV focused beam with $p = 1$ and $m = 1$. The intensity components clearly differ and vary according to the beam parameters. Although both $|E_x|^2$ and $E_y|^2$ appear similar, the intensity of the outer–rings is higher for E_y which is expected according to Eq. 10 and 11. In the case of $|E_z|^2$, the hollow form is wider and the phase is clockwise before the focus plane and changes anticlockwise after the focus plane. The dynamic evolution of the phase profile during propagation before the focal plane is shown in Supplementary Video 1. Additionally, the phase profile during propagation after the focal plane is presented in Supplementary Video 2. In addition, it can be seen that the orbital angular momentum (OAM) of the focused beam

increases from 1 to 2, indicating OAM generation from the spin angular momentum due to spin–orbit interaction. On the other hand, for a right-hand CPLGV focused beam, the OAM decreases by 1 –from 1 to 0– as can be clearly understood from Eq. 9c [19]. Furthermore, in the focal plane, the intensity profile of the CPLGV beam forms rings with wider central hollows compared to those in the near-focus region.

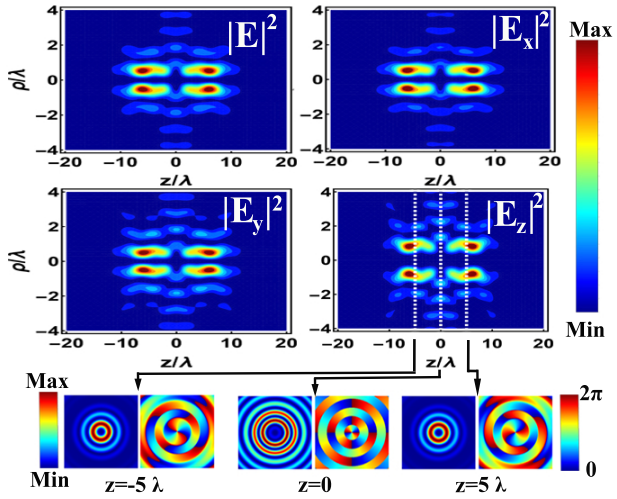

Figure 2. Intensity distribution of the left–handed CPLGV beam $|\mathbf{E}_t|^2$ (A) and the corresponding components $|E_x|^2$ (B), $|E_y|^2$ (C), and $|E_z|^2$ (D) in $\rho - z$ plane with phase and intensity of $|E_z|^2$ at $z = -5\lambda, 0, 5\lambda$ in $x - y$.

Fig. 3 depicts the focus intensity distribution of the left–handed CPLGV beam in the focal region of the binary axicon for different values of the truncation parameter β which takes the values of $\beta = 1.1, 1.5, 2, 2.5, 3$ and 3.5. It can be clearly seen that the intensity distribution changes considerably causing reforming of the focus shape. The intensity at focus $z = 0$ is forming with multi-rings for $\beta = 1.1$ Fig. 3-(A) which become tighter with reforming the whole intensity as shown in Fig. 3-(B). After that, the behaviour changes to form a wide rings with a greater increase in the value of β as clearly shown in Fig. 3-(C), and then changes with increasing of β values, reforming the intensity not only at $z = 0$ but also along the focal region. This is owing to the changes in the intensity of the double–ring incident beam at the aperture plane and the interference of its components.

We now focus on how the optical system parameters influence the focal shaping of the left–handed CPLGV focused beam when focused by the binary axicon. Fig. 4 shows the intensity distributions of CPLGV focused beam in the focal region of the binary axicon for different values of the obstruction parameter δ: (A) $\delta = 0$, (B) $\delta = 0.25$, (C) $\delta = 0.50$ and (D) $\delta = 0.75$.The intensity distribution clearly changes with increasing obstruction. The maximum values of both defocusing and focusing axicons were formed on both sides of focal plane and the focal region decreases as the obstruction increased resulting in changes in the form

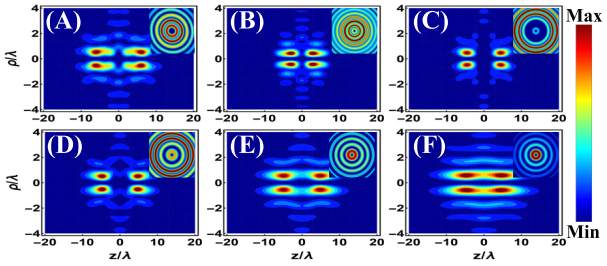

Figure 3. Intensity distribution of the left–handed CPLGV beam in the focal region of the binary axicon for different values of truncation parameter β: (A) $\beta = 1.1$, (B) $\beta = 1.5$, (C) $\beta = 2$, (D) $\beta = 2.5$, (E) $\beta = 3$ and (F) $\beta = 3.5$ with the corresponding intensity distribution at $z = 0$ in the focal plane.

of intensity. For high value of obstruction as shown in Fig. 4-(D), the intensity is divided into multifoci with maximum intensity at the focal plane.

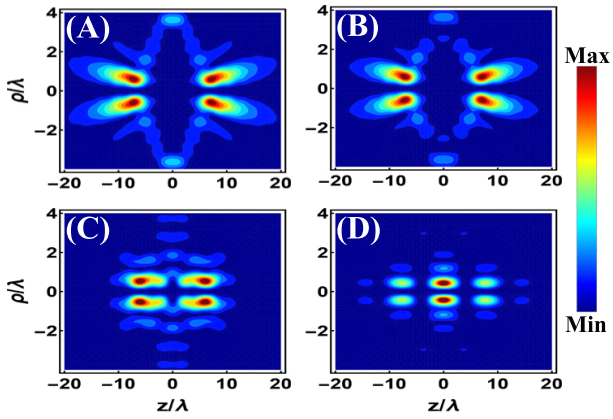

Figure 4. Intensity distribution of the left–handed CPLGV beam in the focal region of the binary axicon for different values of obstruction parameter δ: (A) $\delta = 0$, (B) $\delta = 0.25$, (C) $\delta = 0.50$ and (D) $\delta = 0.75$.

Fig. 5 shows the changes in the intensity distribution of left–handed CPLGV beam with numerical aperture NA. As the NA increases, the focal region becomes tighter, accompanied by changes in the intensity distribution. Furthermore, the focuses of both the positive and negative axicons become tighter and more separated from each other, resulting in changes in the intensity rings both in the focal plane and along the focal region.

4. CONCLUSION

In conclusion, focus shaping of left–hand circularly polarized Laguerre–Gaussain vortex (CPLGV) beams with binary axicons was rigorously analysed using vector diffraction theory. Through systematic variation of beam parameters—namely, the radial index or beam order p, topological charge m, and truncation parameter β – as well as optical system parameters such as numerical aperture NA and obstruction δ, we demonstrated how the focal intensity distribution

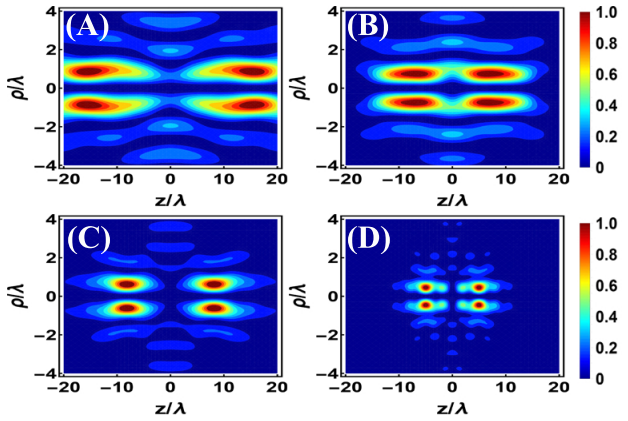

Figure 5. Intensity distribution of the left–handed CPLGV beam in the focal region of the binary axicon for different values of numerical aperture NA: (A) $NA = 0.50$, (B) $NA = 0.60$, (C) $NA = 0.70$ and (D) $NA = 0.90$.

can be significantly altered. The results show that by appropriately tuning these parameters, diverse focal intensity patterns—such as double focal spot, multi foci, and annular focal rings—can be achieved in the focal region of the binary axicon. The OAM of the beam, $m = 1$, increases from 1 to 2 due to spin-to-orbital angular momentum conversion. Increasing the truncation parameter causes reforming of the intensity in the focal region. Additionally, increasing the numerical aperture NA tightens the focal region and separates the contributions of the positive and negative axicons. These results demonstrate the binary axicon's ability to control structured light for advanced beam shaping, with potential applications in trapping and manipulating nanoparticles.

SUPPLEMENTARY MATERIALS

- **Supplementary Video 1:** Phase profile during propagation before focal plane.
- **Supplementary Video 2:** Phase profile during propagation after focal plane.

REFERENCES

[1] L. Allen, M. W. Beijersbergen, R. J. C. Spreeuw, and J. P. Woerdman, "Orbital angular momentum of light and the transformation of laguerre-gaussian laser modes," Phys. Rev. A **45**, 8185–8189 (1992).

[2] A. M. Yao and M. J. Padgett, "Orbital angular momentum: origins, behavior and applications," Adv. Opt. Photon. **3**, 161–204 (2011).

[3] Y. Shen, X. Wang, Z. Xie, *et al.*, "Optical vortices 30 years on: OAM manipulation from topological charge to multiple singularities," Light. Sci. & Appl. **8**, 1–29 (2019).

[4] W. N. Plick and M. Krenn, "Physical meaning of the radial index of Laguerre-Gauss beams," Phys. Rev. A **92**, 063841 (2015).

[5] G. Xie, Y. Ren, Y. Yan, *et al.*, "Experimental demonstration of a 200-gbit/s free-space optical link by multiplexing Laguerre–Gaussian beams with different radial indices," Opt. Lett. **41**, 3447–3450 (2016).

[6] J. Wang, J.-Y. Yang, I. M. Fazal, *et al.*, "Terabit free-space data transmission employing orbital angular momentum multiplexing," Nat. photonics **6**, 488–496 (2012).

[7] M. P. J. Lavery, F. C. Speirits, S. M. Barnett, and M. J. Padgett, "Detection of a spinning object using light's orbital angular momentum," Science **341**, 537–540 (2013).

[8] Z. Guo, Z. Chang, J. Meng, *et al.*, "Generation of perfect optical vortex by Laguerre–Gauss beams with a high-order radial index," Appl. Opt. **61**, 5269–5273 (2022).

[9] Y. Zhang, B. Ding, and T. Suyama, "Trapping two types of particles using a double-ring-shaped radially polarized beam," Phys. Rev. A **81**, 023831 (2010).

[10] A. D. Kiselev and D. O. Plutenko, "Optical trapping by Laguerre-Gaussian beams: Far-field matching, equilibria, and dynamics," Phys. Rev. A **94**, 013804 (2016).

[11] F. M. Thabit and M. A. Shukri, "Trapping of low and high refractive index nano-spherical particles by using a highly focused Laguerre–Gaussian beam," Appl. Opt. **63**, 2614–2620 (2024).

[12] V. Jarutis, R. Paškauskas, and A. Stabinis, "Focusing of laguerre–gaussian beams by axicon," Opt. communications **184**, 105–112 (2000).

[13] Y. Kozawa and S. Sato, "Small focal spot formation by vector beams," Prog. Opt. **66**, 35–90 (2021).

[14] A. A. Alkelly, H. T. Al-Ahsab, M. Cheng, and I. G. H. Loqman, "Tight focusing of azimuthally polarized Laguerre–Gaussian vortex beams by diffractive axicons," Phys. Scripta **99**, 025508 (2024).

[15] Q. Zhan, "Properties of circularly polarized vortex beams," Opt. Lett. **31**, 867–869 (2006).

[16] B. Chen, Z. Zhang, and J. Pu, "Tight focusing of partially coherent and circularly polarized vortex beams," J. Opt. Soc. Am. A **26**, 862–869 (2009).

[17] X. Yin, Z. Zhao, P. Hao, and J. Li, "Spin-orbit interactions of a circularly polarized vortex beam in paraxial propagation," Opt. Express **31**, 1832–1843 (2023).

[18] V. V. Kotlyar, A. A. Kovalev, S. S. Stafeev, and A. M. Telegin, "Orbital angular momentum at the tight focus of a circularly polarized gaussian beam," J. Opt. Soc. Am. A **42**, 52–58 (2025).

[19] H. T. Al-Ahsab, M. Cheng, I. G. H. Loqman, *et al.*, "Focus shaping of circularly polarized Bessel–Gaussian vortex beam with binary axicon for nanoparticle trapping," Opt. Continuum **3**, 1805–1816 (2024).

[20] V. V. Kotlyar, S. S. Stafeev, A. G. Nalimov, *et al.*, "Two-petal laser beam near a binary spiral axicon with topological charge 2," Opt. & Laser Technol. **119**, 105649 (2019).

[21] S. N. Khonina and A. P. Porfirev, "3D transformations of light fields in the focal region implemented by diffractive axicons," Appl. Phys. B **124**, 1–13 (2018).

[22] J. Zhi, Z. Qiu, X. Wang, *et al.*, "Versatile polarization-converted non-diffractive bessel beams based on fully phase-modulated metasurfaces," Opt. Express **32**, 11560–11572 (2024).

[23] X. Pang, W. Liu, and W. Miao, "Generation of spiral spin density vectors with a circularly polarized, vortex beam," IEEE Photonics J. **12**, 1–14 (2019).

[24] W. Yuan, Q. Guo, M. Sang, and Y. Yang, "Flattop shaped creation based on strong focusing of circularly polarized vortex beams," J. Opt. **46**, 164–169 (2017).

[25] J. Wang, F. Li, and G. Kang, "Multiwavelength achromatic super-resolution focusing via a metasurface-empowered controlled generation of focused cylindrically polarized vortex beams," Opt. Express **30**, 30811–30821 (2022).

[26] S. N. Khonina, A. P. Porfirev, S. G. Volotovskiy, *et al.*, "Generation of multiple vector optical bottle beams," Photonics **8** (2021).

[27] I. A. Vovk, A. S. Baimuratov, W. Zhu, *et al.*, "Chiral nanoparticles in singular light fields," Sci. Reports **7**, 45925 (2017).

[28] P. Karpinski, "Rotation and revolution of optically trapped gold nanorods induced by the spin and orbital angular momentum of a Laguerre–Gaussian vortex beam," Adv. Opt. Mater. **10**, 2101592 (2022).

[29] H. Song, K. H. Pae, J. Won, *et al.*, "Characteristics of electron beams accelerated by parallel and antiparallel circularly polarized Laguerre–Gaussian laser pulses," Appl. Phys. B **129**,

56 (2023).
[30] M. Hamidi, A. S. Firouzjaei, and H. Akou, "Enhancing the quality of accelerated electron bunch through the circular laguerre–gauss laser pulses," Braz. J. Phys. **55**, 1–9 (2025).
[31] S. N. Khonina, N. L. Kazanskiy, P. A. Khorin, and M. A. Butt, "Modern types of axicons: new functions and applications," Sensors **21**, 6690 (2021).
[32] I. G. Loqman, A. A. Alkelly, and H. T. Al-Ahsab, "Generating double focal spots by focusing a radially polarized double-ring-shaped beam with an annular classical axicon," Opt. Continuum **1**, 1761–1767 (2022).
[33] S. Khonina, A. Ustinov, S. Kharitonov, *et al.*, "Optical bottle shaping using axicons with amplitude or phase apodization," Photonics **10**, 200 (2023).
[34] J. H. McLeod, "The axicon: A new type of optical element," J. Opt. Soc. Am. **44**, 592–597 (1954).
[35] S. A. M. kaid, H. O. Al-Nadary, M. S. Qusailah, and A. A. Alkelly, "Intensity distribution of the partially coherent gaussian schell vortex beam diffracted by classical axicon," Sana-a Univ. J. Appl. Sci. Technol. **2**, 197–204 (2024).
[36] M. Zhang, X. Liu, L. Guo, *et al.*, "Partially coherent flat-topped beam generated by an axicon," Appl. Sci. **9**, 1499 (2019).
[37] N. Zhang, J.-S. Ye, S.-F. Feng, *et al.*, "Generation of long-distance stably propagating Bessel beams," OSA Continuum **4**, 1223–1233 (2021).
[38] X. Huang, Z. Chang, Y. Zhao, *et al.*, "Generation of the anomalous vortex beam by spiral axicon implemented on spatial light modulator," Front. Phys. **10**, 951516 (2022).
[39] M. M. Sánchez-López, I. Moreno, J. A. Davis, *et al.*, "Double-ring interference of binary diffractive axicons," OSA Continuum **3**, 1679–1690 (2020).
[40] M. Han, D. Smith, T. Kahro, *et al.*, "Extending the depth of focus of an infrared microscope using a binary axicon fabricated on barium fluoride," Micromachines **15** (2024).
[41] S. A. Degtyarev, A. P. Porfirev, and S. N. Khonina, "Photonic nanohelix generated by a binary spiral axicon," Appl. Opt. **55**, B44–B48 (2016).
[42] B. Richards, E. Wolf, and D. Gabor, "Electromagnetic diffraction in optical systems, II. structure of the image field in an aplanatic system," Proc. Royal Soc. London. Ser. A. Math. Phys. Sci. **253**, 358–379 (1959).
[43] T. Zeng and J. Ding, "Three-dimensional multiple optical cages formed by focusing double-ring shaped radially and azimuthally polarized beams," Chin. Opt. Lett. **16**, 031405 (2018).
[44] Y. Zhang, "Generation of three-dimensional dark spots with a perfect light shell with a radially polarized Laguerre–Gaussian beam," Appl. optics **49**, 6217–6223 (2010).
[45] N. Umamageswari, K. Rajesh, M. Udhayakumar, *et al.*, "Tight focusing properties of spirally polarized LG(1, 1)* beam with high na parabolic mirror," Opt. Quantum Electron. **50**, 1–11 (2018).
[46] G. N. Watson, *theory of Bessel functions* (Cambridge U. Press, 1944).